Obrabotka metallov (tekhnologiya, oborudovanie, instrumenty) = Metal Working and Material Science. 2026 vol. 28 no. 2 pp. 223–242
ISSN: 1994-6309 (print) / 2541-819X (online)
DOI: 10.17212/1994-6309-2026-28.2-223-242

NSTU NETI

Obrabotka metallov -
Metal Working and Material Science

Journal homepage: http://journals.nstu.ru/obrabotka_metallov

Formation of a single-phase recrystallized structure in titanium-based alloys with natural Elinvar behavior by thermomechanical processing

Alexandra Baranova [a, *], *Anastasia Skirpichnikova* [b], *Oleg Strakhov* [c], *Andrey Bazlov* [d], *Olga-Lilia Eliseeva* [e], *Sergey Dubinskiy* [f]

National University of Science and Technology MISIS, Leninskiy Prospekt 4, p. 1, Moscow, 119049, Russian Federation

[a] https://orcid.org/0000-0002-1470-4282, baranova.al.pavlovna@yandex.ru; [b] https://orcid.org/0009-0002-1664-7039, skirpichnikova@internet.ru; [c] https://orcid.org/0009-0007-9603-2398, strakhovo2018@gmail.com; [d] https://orcid.org/0000-0002-0409-1056, bazlov@misis.ru; [e] https://orcid.org/0009-0004-2162-2906, eliseeva.olli@gmail.com; [f] https://orcid.org/0000-0002-5719-5932, dubinskiy.sm@misis.ru

ARTICLE INFO

Article history:
Received: 26 January 2026
Revised: 04 February 2026
Accepted: 14 March 2026
Available online: 15 June 2026

Keywords:
Titanium alloys
Elinvar alloys
Thermomechanical processing
Longitudinal rolling
Cold rolling
Hot rolling
Structure formation
Phase analysis

Funding
The present work was carried out with the financial support of the Russian Science Foundation, Project No. 25-73-10041, https://rscf.ru/project/25-73-10041/.

ABSTRACT

Introduction. The development of a new class of non-magnetic corrosion-resistant materials with constant elastic properties over a wide temperature range — i.e., exhibiting *Elinvar* effect — is a pressing challenge in the transition to advanced intelligent manufacturing technologies and robotic systems. To address this challenge, it is necessary to develop a process chain for producing ingots of stable β-titanium alloys with *Elinvar* effect. Achieving a stable recrystallized structure of the alloys over a wide temperature range also appears promising. Such advances will enable the use of this class of materials in the fabrication of elastic elements intended for oscillatory measuring systems in aerospace and other high-tech applications. ***Purpose.*** This study aimed to investigate the feasibility of producing a recrystallized β-phase structure in *Ti–Nb–Zr*, *Ti–Nb*, and *Ti–Mo* alloys exhibiting a new type of *Elinvar* behavior using thermomechanical processing methods. To achieve this purpose, the following tasks were accomplished: (1) production of ingots of stable β-titanium potentially Elinvar alloys *Ti–22Nb–15Zr*, *Ti–40Nb*, *Ti–45Nb*, *Ti–50Nb*, *Ti*–12.6*Mo*, *Ti–15Mo*, and *Ti–20Mo* (at.%); (2) development of a processing sequence capable of forming a recrystallized equiaxed β-phase structure without traces of other phases, given that the new type of *Elinvar* behavior is structurally insensitive; and (3) investigation of the structural and phase state of alloys with potentially natural *Elinvar* behavior, and elucidation of the relationship between grain size and alloying element content. **Methods.** The objects of the study were ingots of *Elinvar* alloys *Ti–22Nb–15Zr*, *Ti–40Nb*, *Ti–45Nb*, *Ti–50Nb*, *Ti*–12.6*Mo*, *Ti–15Mo*, and *Ti–20Mo* (at.%). The ingots were smelted in an electric arc furnace with a tungsten electrode. The samples were then subjected to thermomechanical processing according to the following schedule: longitudinal hot rolling (true logarithmic strain $e = 0.3$), homogenization annealing, longitudinal cold rolling (true logarithmic strain $e = 0.67$), and post-deformation annealing. Annealing was performed at 1,000 °C for 30 minutes in an argon atmosphere, followed by water quenching. The structural and phase state of the samples was investigated using optical and electron microscopy, X-ray diffraction (*XRD*), and energy-dispersive X-ray spectroscopy (*EDS*). The average grain size was determined using the linear intercept method. **Results and discussion.** Stable β-titanium *Elinvar* alloy ingots were obtained. They are characterized by a high degree of chemical homogeneity and compliance with the specified composition throughout the cross-section. It was found that the proposed thermomechanical processing route for these alloys leads to the formation of a single-phase recrystallized structure consisting of equiaxed β-phase grains. Grain sizes are shown to vary from 22.6 ± 1.4 to 68.1 ± 3.7 μm. In binary alloys of the *Ti–Nb* and *Ti–Mo* systems, a decrease in grain size is observed with an increase in the *Nb* and *Mo* content. Specifically, for the *Ti–Nb* system, the grain size decreased from 57.8 ± 3.3 μm to 22.6 ± 1.4 μm with an increase in niobium content of 10 at.%. For the *Ti–Mo* system, the grain size decreased from 68.1 ± 3.7 μm to 34.4 ± 2.0 μm with an increase in molybdenum content of 7.4 at.%. The formation of a recrystallized equiaxed β-phase structure throughout the ingot volume during combined thermomechanical processing confirms the potential for industrial application of these alloys.

For citation: Baranova A.P., Skirpichnikova A.A., Strakhov O.V., Bazlov A.I., Eliseeva O.-L.V., Dubinskiy S.M. Formation of a single-phase recrystallized structure in titanium-based alloys with natural Elinvar behavior by thermomechanical processing. *Obrabotka metallov (tekhnologiya, oborudovanie, instrumenty) = Metal Working and Material Science*, 2026, vol. 28, no. 2, pp. 223–242. DOI:10.17212/1994-6309-2026-28.2-223-242. (In Russian).

Introduction

In conventional metals and alloys, *Young's* modulus (***E***) generally decreases with increasing temperature. However, certain materials exhibit an anomalous elastic behavior characterized by a very low temperature sensitivity of the elastic modulus and an almost constant value within a limited temperature range. Such

*** Corresponding author**
Baranova Alexandra P., Ph.D. (Physics and Mathematics), Senior researcher
National University of Science and Technology MISIS,
Leninskiy Prospekt 4, p. 1,
119049, Moscow, Russian Federation
Tel.: +7 999 924-08-09, **e-mail**: baranova.al.pavlovna@yandex.ru

behavior was first reported in 1920 by the *Swiss–French* physicist *C. E. Guillaume* in an *Fe–Ni–Cr* alloy system and was termed *Elinvar* behavior [1, 2].

Elinvar alloys are widely used for the fabrication of components of oscillatory measuring systems requiring constant elastic properties over the operational temperature range, including microelectromechanical systems (*MEMS*) employed in miniature sensors and transducers [3–6]. Sensors manufactured from *Elinvar* alloys, in addition to their direct aerospace applications, can also be utilized in robotics and other high-technology fields where high measurement accuracy is required [7]. A key advantage of *Elinvar* alloys is the possibility of creating medium-precision inertial sensors based on ring, cylindrical, and bell-shaped resonators [7].

Elinvar behavior is typically characterized by a temperature coefficient of the elastic modulus on the order of 10^{-5}–10^{-6} °C^{-1} [2, 8, 9]. Several mechanisms explaining the origin of *Elinvar* behavior have been proposed in the literature, including mechanisms associated with magnetic moment interactions [2, 8, 9], phase transformations and pre-transitional phenomena [10–13], high dislocation density [10, 14], and anisotropy of temperature dependencies of elastic constants in low-symmetry crystal lattices [13, 15–22].

However, recently a new type of *Elinvar* behavior has been discovered, which is associated with a unique interatomic interaction in the *BCC* **β**-phase of titanium alloys [23, 24]. This type of *Elinvar* behavior is distinguished by a wide temperature range (up to ~400 °C), low sensitivity to the structural state of the alloy, and insensitivity to external magnetic fields.

Such behavior was first observed in the shape memory alloy *Ti-22 Nb-6 Zr* (at.%) during cooling from the high-temperature **β**-phase stability region in the temperature range from 550 to 150 °C [18,19]. However, the practical implementation of the *Ti-22 Nb-6 Zr* alloy is limited by several factors. These include premartensitic phenomena occurring near room temperature, which are accompanied by a decrease in the elastic modulus below 150 °C, and the precipitation of the isothermal **ω**-phase during heating, which leads to a significant change in the elastic modulus and, consequently, the loss of *Elinvar* behavior [23, 24].

An increase in the heating rate can suppress the precipitation of the **ω**-phase; however, this approach makes the alloy sensitive to the heating rate and therefore imposes limitations on its operational parameters [25, 26]. Suppression of premartensitic phenomena by lowering the martensitic transformation temperature and the premartensitic softening range can be achieved by additional alloying with zirconium [27]. In particular, the alloy composition *Ti-22 Nb-15 Zr* exhibits martensitic transformation start temperatures and premartensitic phenomena approximately 315 °C lower than those observed in *Ti-22 Nb-6 Zr*.

Subsequently, a new type of *Elinvar* behavior was also observed in the stable **β**-titanium alloy *Ti-50 Nb*, where it manifests itself in two temperature ranges extending up to 200 °C and separated by a temperature region in which *Elinvar* behavior is absent [28]. Based on the phase diagram [29] and [30], alloys containing at least 40 at.% *Nb* are classified as stable **β**-alloys.

At lower niobium contents, precipitation of the stable **α**-phase as well as metastable phases such as **α′** and **α″-martensite**, $\boldsymbol{\omega}_{iso}$, and $\boldsymbol{\omega}_{ath}$ can occur [31–35]. All of this confirms the promising potential of searching for alloy compositions exhibiting the new type of *Elinvar* behavior among stable **β**-titanium alloys [36]. Alloys of the *Ti–Mo* system are also promising candidates, since molybdenum is a stronger **β**-stabilizer than niobium. As shown in [37–39], alloying titanium with approximately 30 at.% *Mo* is sufficient to obtain a stable **β**-phase alloy. Moreover, some studies report the formation of a relatively stable **β**-phase even at a molybdenum content as low as 12.6 at.% *Mo* [40]. Such relatively low alloying levels allow most lattice sites in the crystal structure to remain occupied by titanium atoms, whose interatomic interactions in the **β**-phase are responsible for the new type of *Elinvar* behavior. Therefore, stable **β**-titanium alloys of the *Ti–Nb* and *Ti–Mo* systems appear to be promising candidates for the development of materials exhibiting the new type of *Elinvar* behavior [23, 24].

Since the new type of *Elinvar* behavior originates from interatomic interactions and is practically independent of the grain structure of the alloy, the formation of a stable recrystallized microstructure over a wide temperature range appears promising from the viewpoint of practical applications [30].

Traditionally, titanium alloys are subjected to hot rolling followed by homogenization after melting in order to eliminate casting defects and facilitate subsequent thermomechanical processing (*TMP*) [41, 42].

The degree of hot rolling is typically no less than 25% (true logarithmic strain ***e*** ≈ 0.3), while the temperatures of hot rolling and homogenization annealing are varied within 850–1,200 °C, depending on the alloy composition, in order to avoid the **β** → **α** transformation [41–45]. To obtain a recrystallized microstructure, *TMP* is employed, which involves cold rolling followed by recrystallization annealing [28, 46, 47].

For ternary alloys of the *Ti–Nb–Zr* system, compositions close to *Ti-22 Nb-15 Zr* are typically subjected to cold longitudinal rolling with a true strain **ε** ranging from 0.2 to 2.9, followed by recrystallization annealing at 550–900 °C for 5–60 min, resulting in a recrystallized **β**-phase microstructure with grain sizes of 50–150 μm [28, 46, 47].

The *Ti-50 Nb* alloy was subjected to *TMP*, consisting of hot longitudinal rolling at 900 °C with **ε** = 0.3, followed by post-deformation annealing (*PDA*) at 1,000 °C for 10 min. This resulted in the formation of a recrystallized single-phase **β** structure [28, 29]. For alloys of the *Ti–Mo* system, however, information on TMP remains limited. Available data are mainly restricted to homogenization annealing. For example, the *Ti-17.6 Mo* alloy was homogenized at 1,000 °C for 6 h followed by water quenching, resulting in an equiaxed **β**-phase microstructure without reported grain size data [48]. In the case of the *Ti-12.6 Mo* alloy, homogenization annealing at 1,000 °C for 1 h, followed by hot rolling at 900 °C, air cooling, and subsequent annealing at 900 °C for 1 h with water quenching, produced a recrystallized single-phase **β-**structure with grain sizes exceeding 100 μm [40, 49].

However, systematic studies addressing the possibility of thermomechanical processing (*TMP*) and the formation of a recrystallized **β**-phase in titanium alloys exhibiting the new type of *Elinvar* behavior are currently lacking.

Therefore, ***the purpose of this work*** was to investigate the possibility of forming a recrystallized **β**-phase microstructure in titanium alloys of the *Ti–Nb–Zr*, *Ti–Nb*, and *Ti–Mo* systems exhibiting the new type of *Elinvar* behavior using thermomechanical processing.

To achieve this purpose, ***the following research objectives*** were addressed:

– to produce ingots of stable **β-**titanium alloys with potential *Elinvar* behavior: *Ti-22 Nb-15 Zr*, *Ti-40 Nb*, *Ti-45 Nb*, *Ti-50 Nb*, *Ti-12.6 Mo*, *Ti-15 Mo*, and *Ti-20 Mo*;

– to develop a *TMP* route enabling the formation of a recrystallized equiaxed **β-**phase microstructure free of secondary phases;

– to investigate the structural and phase states of alloys exhibiting potential intrinsic *Elinvar* behavior and to determine the relationship between grain size and alloying element content.

Methods

The *Ti-22 Nb-15 Zr*, *Ti-40 Nb*, *Ti-45 Nb*, *Ti-50 Nb*, *Ti-12.6 Mo*, *Ti-15 Mo*, and *Ti-20 Mo* (at.%) alloys were selected as potentially promising materials exhibiting a new type of *Elinvar* behavior. Ingots weighing 50 g were produced by arc melting in an *Arcast Arc 200* laboratory furnace (*Arcast Inc.* , USA) using a non-consumable tungsten electrode in an argon atmosphere. A similar ingot production procedure was employed as shown in [19, 30]. Cp-titanium wire (*VT1-00* grade), cp-niobium wire (*NB-1* grade), cp-molybdenum wire (*MCh* grade), and iodide zirconium were used as starting materials. The starting materials were mechanically crushed to a fraction size below 5 mm in their largest dimension. To ensure chemical homogeneity, the ingots were subjected to six consecutive remelts. The correspondence to the target composition, as well as the homogeneity of the distribution of the major elements, was assessed by energy-dispersive X-ray spectroscopy (*EDS*) using a *Tescan Vega3 SBH* scanning electron microscope (*TESCAN*, Czech Republic) in two regions, namely the edge and the center. The relative measurement error did not exceed ±1.0%. To evaluate chemical homogeneity, the analysis was carried out in two areas across the cross-section of each ingot. The selection of these two areas was dictated by the need to identify possible segregation during solidification. In each area, measurements were performed at five points. The content of gas-forming impurities was evaluated by the reductive melting method using a *TC-600* analyzer (*Leco*, the Netherlands).

After melting, rectangular billets with dimensions of 25–30 × 9–10 mm and a length of 38–43 mm were cut from the ingots by electrical discharge machining and were subsequently subjected to *TMP*. The

TMP route included longitudinal hot rolling, homogenization annealing, longitudinal cold rolling, and *PDA* (post-deformation annealing). The general *TMP* scheme is shown in Fig. 1.

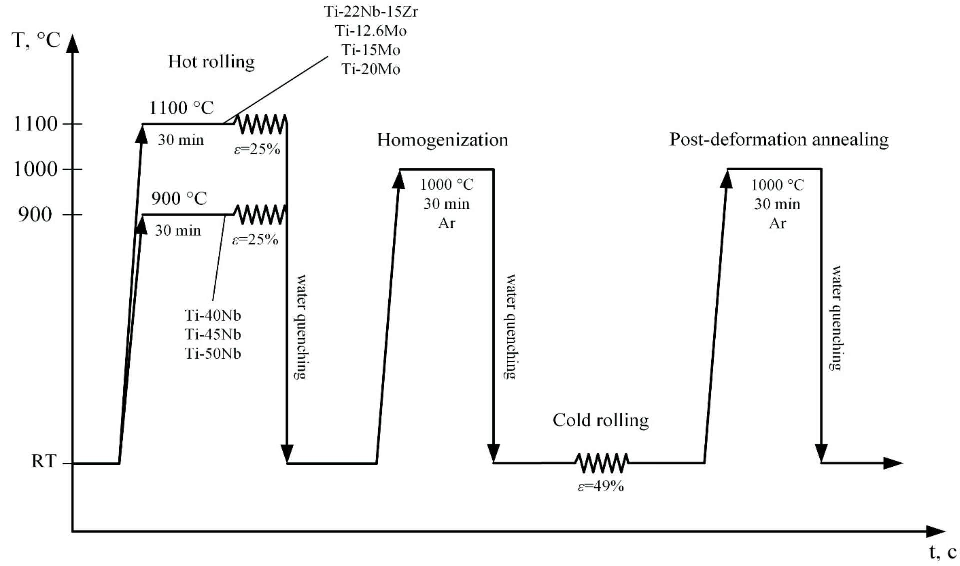

Fig. 1. Schematic of the thermomechanical processing route for Elinvar alloys

Hot rolling was carried out to eliminate defects of the cast structure. Prior to rolling, the billets were placed in a laboratory furnace *SNOL-4* and then heated to 900 °C for the *Ti-40 Nb*, *Ti-45 Nb*, and *Ti-50 Nb* alloys, and to 1,100 °C for the *Ti-22 Nb-15 Zr*, *Ti-12.6 Mo*, *Ti-15 Mo*, and *Ti-20 Mo* alloys, followed by a holding time of 30 min to ensure uniform heating throughout the entire cross-section. The heating temperature and holding time were selected based on phase diagram data [29] so that the alloys were in the single-phase **β-**region during processing.

The rolling process was carried out on a *DUO-210* rolling mill in a single pass, with a reduction of 25% (true logarithmic strain $\boldsymbol{e}$ = 0.3).

After rolling, the specimens were water quenched in order to stabilize the structure and to suppress the precipitation of isothermal phases that could form during slow cooling.

After hot rolling, the billets were subjected to homogenization annealing in a protective argon atmosphere at 1,000 °C in a *UPP-200M* quenching furnace (*YASAM*, Russia) in order to obtain a chemically homogeneous composition and to complete recrystallization processes initiated during hot rolling. For this purpose, the specimens were placed into a preheated furnace, held for 30 min, and subsequently quenched in water.

Following homogenization, the billets were cut by electrical discharge machining into specimens with a rectangular cross-section of 5 × 6–7 × 45–52 mm, which were then subjected to cold rolling. The specimens were rolled in 10 passes with a total reduction of **ε** = 49% (true logarithmic strain $\boldsymbol{e}$ = 0.67) using *Chinetti LM120* electromechanical stationary rolling mills (*Chinetti snc*, Italy).

To form a recrystallized structure, the billets after rolling were subjected to *PDA* at 1,000 °C in an argon atmosphere using a *UPP-200M* quenching furnace (*YASAM*, Russia). The billets were placed in a furnace preheated to 1,000 °C, held for 30 min, and subsequently quenched in water. The annealing temperature was selected so that recrystallization proceeded within the single-phase **β**-region.

After *TMP*, the phase composition was studied using a *DRON-4* X-ray diffractometer (Russia) with *CuK*α radiation in the range of 30–100°, with an exposure time of 3 s and a scanning step of 0.05°. The tube operating parameters were $\boldsymbol{U}$ = 49 kV and $\boldsymbol{I}$ = 30 mA. Specimens with dimensions of 7 × 7 mm were cut using a diamond disk and subsequently ground with abrasive papers of *P120–P1,200* grit size, followed by chemical etching to remove the deformed and oxidized surface layer. The following etching solutions were used:

– $1HF : 3HNO_3 : 6H_2O$ for the *Ti-22 Nb-15 Zr* alloy;
– $1HF : 3HNO_3 : 10H_2O$ for the *Ti-40 Nb*, *Ti-45 Nb*, and *Ti-50 Nb* alloys;
– $1HF : 3HNO_3 : 16H_2O$ for the *Ti-12.6 Mo*, *Ti-15 Mo*, and *Ti-20 Mo* alloys.

The grain structure of the alloys was investigated by optical microscopy using a *ZEISS Axio Observer* metallographic optical microscope (*Zeiss*, Germany) equipped with *Tixomet Pro* software. The specimens were prepared using a procedure similar to that employed for X-ray diffraction specimens. The difference was that grinding was performed using abrasive papers with grit sizes up to *P4,000*, followed by polishing with a 0.05 μm silicon oxide suspension and a 3% hydrogen peroxide solution. Chemical etching was then carried out until the grain structure became visible.

The average grain size was determined using the random intercept method. To obtain statistically reliable results, at least 300 intercepts were measured for each specimen. Statistical processing of the grain size measurements was performed using *Student's t*-test with a 95% confidence level $\boldsymbol{t} = 1.967$.

Results and Discussion

Production and characterization of alloy ingots

The typical appearance of the *Elinvar* alloy ingots after melting is shown in Fig. 2. The ingots exhibit a luster without discoloration, significant pores, or shrinkage cavities.

The results of the quantitative chemical analysis, presented in Table 1, indicate a homogeneous distribution of the main elements across the ingot cross-section and confirm agreement with the target compositions within the accuracy of the method. Elemental distribution maps (Fig. 3) demonstrate a high degree of homogeneity of the main elements throughout the ingot volume.

Fig. 2. Typical appearance of ingots after smelting

Table 1

Chemical composition of the main elements in the alloys

Alloy	Zone	Chemical element (at. %)			
		Ti	*Nb*	*Mo*	*Zr*
Ti–22 Nb–15 Zr	edge	62.6	21.9	–	15.5
	center	62.0	22.4	–	15.6
Ti–40 Nb	edge	58.3	41.7	–	–
	center	60.1	39.9	–	–
Ti–45 Nb	edge	55.2	44.8	–	–
	center	55.2	44.8	–	–
Ti–50 Nb	edge	49.7	50.3	–	–
	center	50.7	49.3	–	–
Ti–12.6 Mo	edge	887.0	–	13.0	–
	center	87.2	–	12.8	–
Ti–15 Mo	edge	85.1	–	14.9	–
	center	84.2	–	15.8	–
Ti–20 Mo	edge	80.5	–	19.5	–
	center	79.5	–	20.5	–

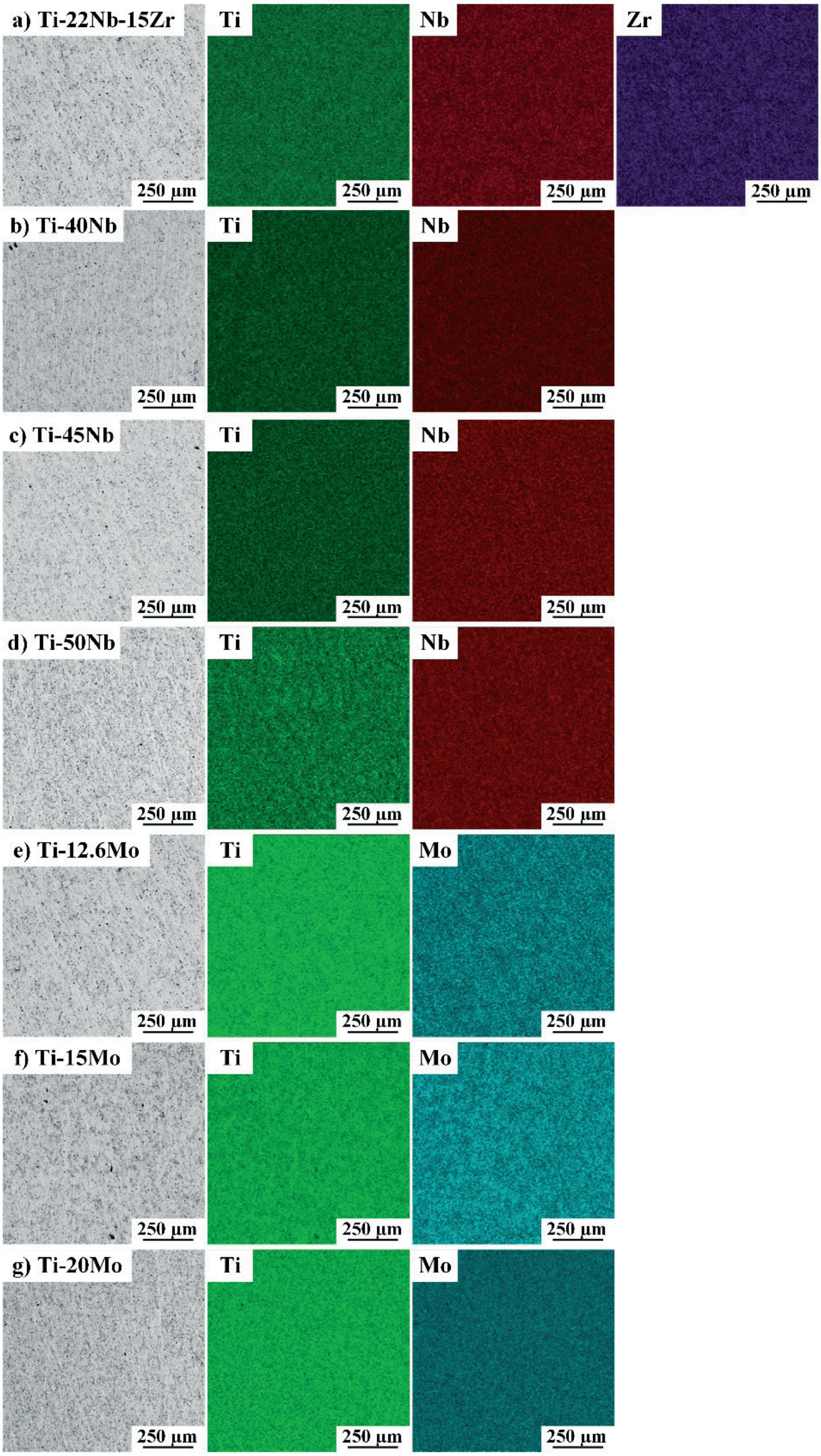

Fig. 3. Distribution maps of the main elements in ingots of Elinvar alloys:
a – Ti–22Nb–15Zr; *b* – Ti–40Nb; *c* – Ti–45Nb; *d* – Ti–50Nb; *e* – Ti–12.6Mo; *f* – Ti–15Mo and *g* – Ti–20Mo

The content of gas-forming impurities was determined to be $O = 0.143 \pm 0.002$ wt.%, $N < 0.016$ wt.%, and $H < 0.0039 \pm 0.0004$ wt.% for all ingots, which meets the requirements of *GOST* standards for industrial titanium alloys [50].

After melting, the ingots were subjected to longitudinal hot rolling. Hot rolling was performed with a true logarithmic strain of $\boldsymbol{e} = 0.3$, which was selected based on the data presented in [51] as sufficient for eliminating the cast structure. The hot rolling temperatures were chosen individually for each alloy group based on previous study and the phase diagrams of the *Ti–Nb*, *Ti–Mo*, and *Ti–Nb–Zr* systems. For the binary alloys *Ti–40 Nb*, *Ti–45 Nb*, and *Ti–50 Nb*, a rolling temperature of 900 °C was selected based on [28], whereas for the alloys *Ti–22 Nb–15 Zr*, *Ti–12.6 Mo*, *Ti–15 Mo*, and *Ti–20 Mo*, a temperature of 1,100 °C was applied based on [29, 35].

The appearance of the billets of the potential *Elinvar* alloys after longitudinal hot rolling is shown in Fig. 4.

After longitudinal hot rolling, the billets of the *Elinvar* alloys were subjected to homogenization annealing at 1,000 °C for 30 min in order to complete the homogenization processes and finalize recrystallization processes that had occurred dynamically during hot rolling. Such a unified annealing route was selected for all alloys as it corresponds to the single-phase **β**-region in terms of temperature and provides sufficient time for diffusion processes during homogenization, based on [28, 29, 40, 42, 52, 53] (Fig. 5).

Subsequently, the alloys were subjected to longitudinal cold rolling with a true logarithmic strain of $\boldsymbol{e} = 0.67$. According to [43, 46, 51], this level of deformation is sufficient to initiate subsequent recrystallization processes during annealing, while remaining moderate and therefore not leading to severe material damage.

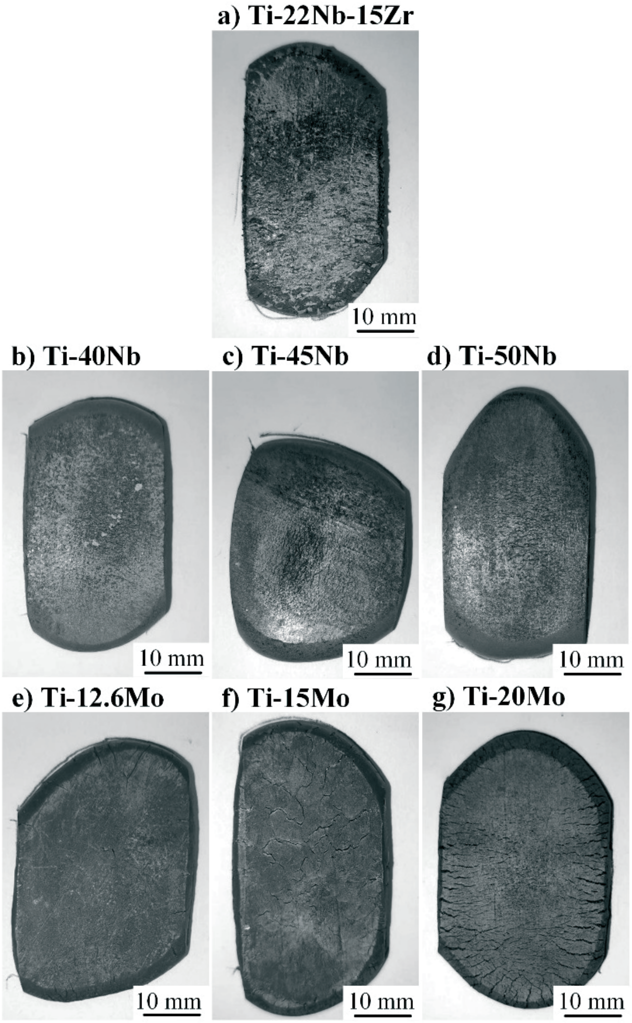

Fig. 4. Blanks of Elinvar alloys after longitudinal hot rolling

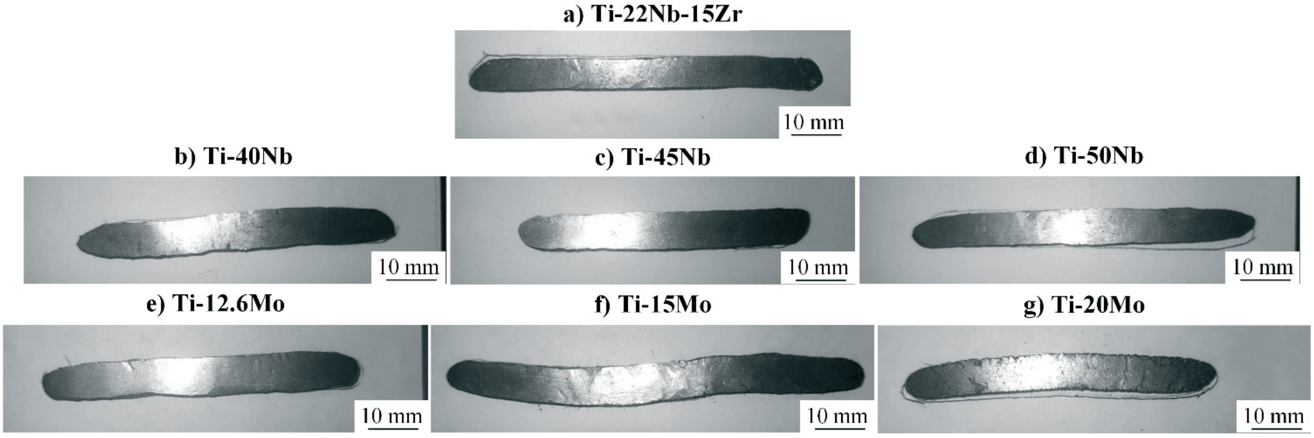

Fig. 5. Blanks of Elinvar alloys after longitudinal cold rolling

After cold rolling, the alloys were subjected to recrystallization annealing under conditions similar to those used for homogenization annealing, since such a route ensures recrystallization of the alloys within the single-phase **β**-region.

It should be noted that the billets of all investigated alloys – *Ti–22 Nb–15 Zr*, *Ti–40 Nb*, *Ti–45 Nb*, *Ti–50 Nb*, *Ti–12.6 Mo*, *Ti–15 Mo*, and *Ti–20 Mo* – successfully passed through all stages of *TMP*, including longitudinal hot and cold rolling with intermediate *PDA*, without significant cracking or the formation of pronounced edge cracks. This indicates the feasibility of applying *TMP*, particularly the routes used in the present study, for the production of *Elinvar* alloys.

Investigation of the phase and microstructural state after TMP

The X-ray diffractograms of the Elinvar alloys *Ti–22 Nb–15 Zr*, *Ti–40 Nb*, *Ti–45 Nb*, *Ti–50 Nb*, *Ti–12.6 Mo*, *Ti–15 Mo*, and *Ti–20 Mo* obtained after *TMP* are presented in Fig. 6. The phase composition of all investigated alloys is represented exclusively by the *BCC* **β**-phase. No diffraction peaks corresponding to other phases were detected.

The absence of secondary phases, apart from the primary **β**-phase, indicates that the *PDA* temperature and subsequent cooling rate were appropriately selected. This phase state was ensured by quenching all investigated alloys from the single-phase region. Such a phase composition, consisting solely of the **β**-phase, is a necessary condition for the realization of the new type of *Elinvar* behavior [24, 28].

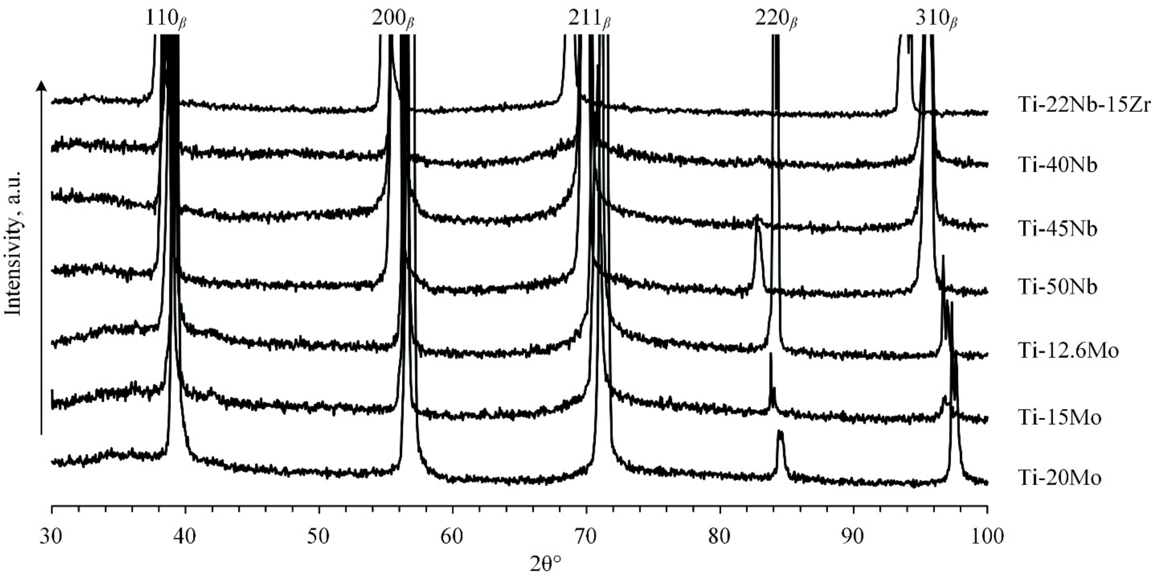

Fig. 6. X-ray diffraction patterns of Elinvar Ti–22 Nb–15 Zr, Ti–40 Nb, Ti–45 Nb, Ti–50 Nb, Ti–12.6 Mo, Ti–15 Mo and Ti–20 Mo alloys after thermomechanical processing

The results of optical microscopy of the *Ti–22 Nb–15 Zr, Ti–40 Nb, Ti–45 Nb, Ti–50 Nb, Ti–12.6 Mo, Ti–15 Mo and Ti–20 Mo* alloys after *TMP* are presented in Fig. 7. In all alloys, the microstructure consists of equiaxed **β**-phase grains.

No traces of secondary phases or cracks are observed in the microstructure images, despite the presence of etching artifacts and surface relief on some specimens. Based on the obtained microstructure images, the grain sizes were measured using the random intercept method. Subsequently, grain size distribution histograms for the *Elinvar* alloys were constructed from the obtained data, as shown in Fig. 8.

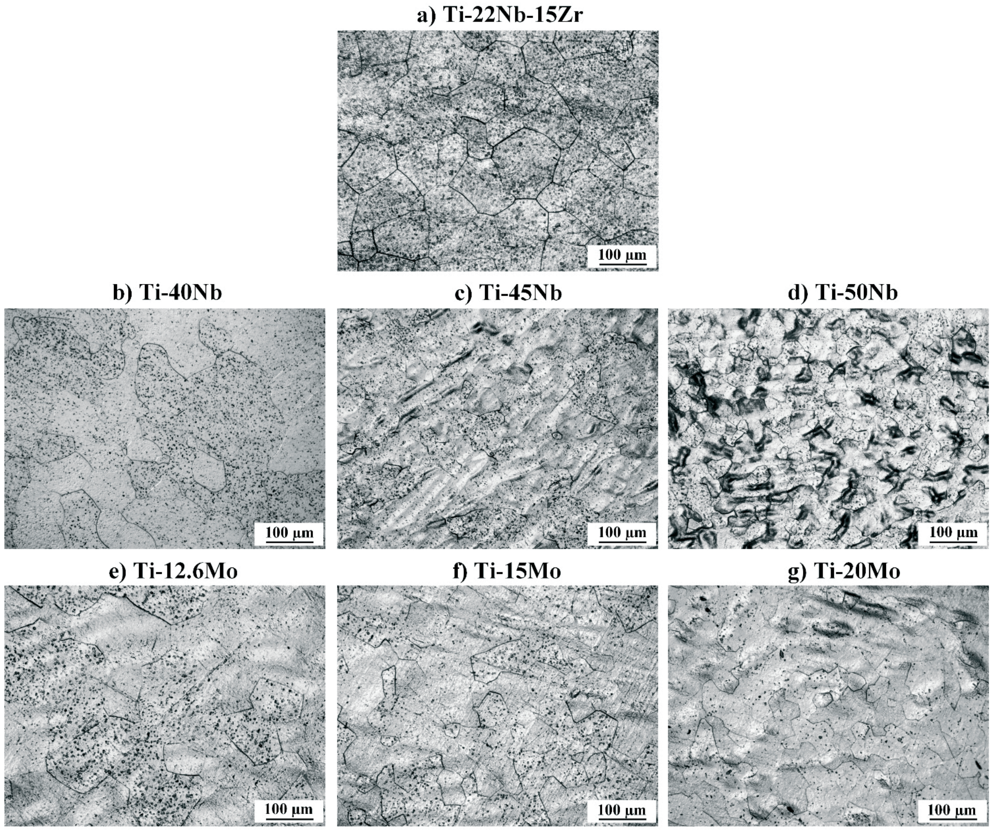

Fig. 7. Microstructure of Elinvar alloys Ti–22 Nb–15 Zr, Ti–40 Nb, Ti–45 Nb, Ti–50 Nb, Ti–12.6 Mo, Ti–15 Mo and Ti–20 Mo

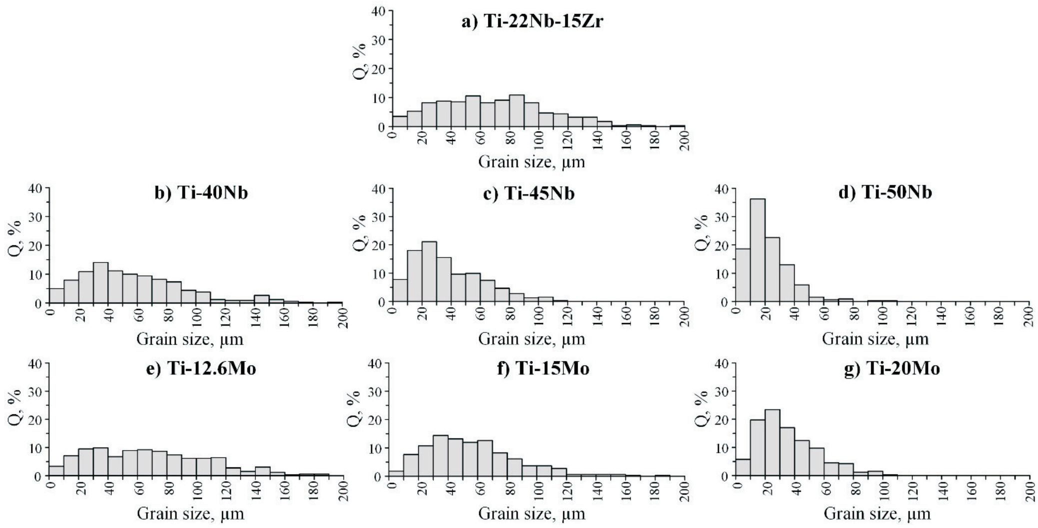

Fig. 8. Grain size distribution histograms of Elinvar alloys Ti–22 Nb–15 Zr, Ti–40 Nb, Ti–45 Nb, Ti–50 Nb, Ti–12.6 Mo, Ti–15 Mo and Ti–20 Mo

The presence of a unimodal distribution in the histograms indicates that primary recrystallization occurred without transition to the grain growth stage, i.e., without secondary recrystallization. This observation confirms that the selected *TMP* route was appropriate for the formation of a homogeneous equiaxed microstructure in the investigated alloys.

The average grain size values in *Elinvar* alloys were calculated based on the analysis of the grain size distribution histograms. The obtained grain size values are presented in Table 2.

Table 2

Average grain size values in *Elinvar* alloys after thermomechanical processing

Alloy	Grain size (μm)
Ti–22 Nb–15 Zr	67.9 ± 3.4
Ti–40 Nb	57.8 ± 3.3
Ti–45 Nb	37.3 ± 2.3
Ti–50 Nb	22.6 ± 1.4
Ti–12.6 Mo	68.1 ± 3.7
Ti–15 Mo	56.3 ± 2.9
Ti–20 Mo	34.4 ± 2.0

In the *Ti-22 Nb-15 Zr* alloy, a recrystallized structure with a grain size of 65–70 μm is formed. In the binary alloys of the *Ti–Nb* and *Ti–Mo* systems, a decrease in grain size is observed with increasing *Nb* and *Mo* content. For example, in the *Ti-40 Nb* alloy, recrystallization results in a microstructure with a grain size of 57.8 ± 3.3 μm. Increasing the *Nb* content by 5 and 10 at. % leads to grain refinement by factors of 1.6 and 2.5, respectively, resulting in grain sizes of 35–40 μm and 19–24 μm.

In the *Ti-12.6 Mo* alloy, a recrystallized microstructure with a grain size of 68.1 ± 3.7 μm is formed. Increasing the *Mo* concentration from 12.6 to 15 and 20 at. % leads to a reduction in the average grain size by factors of 1.2 and 2.0, reaching 53–59 μm and 32–37 μm, respectively. It should be noted that in both binary *Elinvar* alloy systems, a decrease in *Nb* and *Mo* content by 5 at. % results in an approximately 1.6-fold increase in grain size.

The observed effect can be explained in terms of the activation energy of grain growth. For alloys of the *Ti–Mo* system, increasing the molybdenum content from 4 to 20 wt. % leads to a threefold increase in the activation energy of grain growth [54]. An increase in the concentration of the alloying element slows down atomic diffusion, which hinders grain boundary migration [55]. Consequently, in alloys of the *Ti–Mo* and *Ti–Nb* systems, a higher degree of alloying reduces the diffusion mobility of atoms, resulting in the formation of finer grains in more highly alloyed compositions.

The results of the phase and microstructural analysis are in good agreement with the available literature data. In most titanium alloys, *TMP* involving moderate or severe cold rolling followed by *PDA* at temperatures above 700–900 °C allows the formation of a recrystallized **β**-phase microstructure [56–58]. It should be noted that the formation of a recrystallized structure is determined by the combined effect of two factors. The first is the structural insensitivity of the new *Elinvar* mechanism, which is based on a unique interatomic interaction in the *BCC* **β**-phase of titanium alloys [23, 24]. This feature eliminates the need to select a specific *TMP* route aimed at obtaining a particular grain or subgrain size, or even a certain amount of dispersed secondary phases, as required in some other alloy systems [59–61].

The second factor is the high stability of the recrystallized structure during repeated heating and cooling cycles within the temperature range below the final annealing temperature, which should not initiate polygonization or secondary recrystallization processes.

In addition, the deformation levels and temperatures, and annealing parameters used in the present work are technologically feasible under industrial conditions and can be incorporated into real manufacturing processing routes, with minor adjustments related to possible changes in the deformation scheme when producing not flat, but, for example, cylindrical billets [62, 63].

Thus, the structural states of the investigated alloys represented by the single-phase **β**-structure appear promising for further studies of the *Elinvar* behavior using both physical and mechanical characterization methods.

Conclusion

Studies of the phase and microstructural state of alloys with potential intrinsic Elinvar behavior subjected to *TMP* according to the following route were carried out: longitudinal hot rolling, homogenization annealing, longitudinal cold rolling, and post-deformation annealing. Based on the results obtained, the following conclusions can be drawn:

1. Ingots of stable **β**-titanium *Elinvar* alloys *Ti–22 Nb–15 Zr, Ti–40 Nb, Ti–45 Nb, Ti–50 Nb, Ti–12.6 Mo, Ti–15 Mo and Ti–20 Mo* were successfully produced, exhibiting high chemical homogeneity and good agreement with the nominal chemical composition throughout the ingot cross-section.

2. It was established that longitudinal hot rolling with a true logarithmic strain of ***e*** = 0.3 at 1,100 °C for *Ti–22 Nb–15 Zr*, *Ti–12.6 Mo*, *Ti–15 Mo*, and *Ti–20 M*o alloys, and at 900 °C for *Ti–40 Nb*, *Ti–45 Nb*, and *Ti–50 Nb* alloys, enables the production of technologically processable potential *Elinvar* alloys capable of withstanding subsequent thermomechanical processing steps without significant cracking.

3. Based on the phase analysis of the *Elinvar* alloy ingots by X-ray diffraction, it was established that after longitudinal cold rolling with a true logarithmic strain of ***e*** = 0.67 and post-deformation annealing at 1,000 °C for 30 min, the phase composition of the *Elinvar* alloys is represented by a stable **β**-phase. This indicates that the selected *TMP* route effectively suppresses the formation and growth of isothermal phases in alloys with the selected **β**-stabilizer content.

4. Optical microscopy revealed that the microstructure of the *Elinvar* alloys after cold rolling and post-deformation annealing consists of recrystallized equiaxed grains with sizes of 65–70 μm for *Ti–22 Nb–15 Zr*, 21–58 μm for the *Ti–(40–50) Nb* system, and 32–72 μm for the *Ti–(12.6–20) Mo* system. In the binary alloys of the *Ti–Nb* and *Ti–Mo* systems, a decrease in grain size is observed with increasing *Nb* and *Mo* content, which can be related to an increase in the activation energy of grain growth with increasing alloying element concentration. In particular, an increase in *Nb* and *Mo* concentration by 5 at. % leads to a 1.6-fold reduction in grain size.

5. The developed technological processing route, which ensures the formation of a recrystallized equiaxed **β**-phase microstructure through combined *TMP*, opens up possibilities for the potential industrial application of these alloys.

References

1. Scott H. *Relation of the high-temperature treatment of high-speed steel to secondary hardening and red hardness*. Washington, US Government Printing Office Publ., 1920. 46 p.

2. Cahn R.W. An unusual Nobel Prize. *Notes and Records of the Royal Society*, 2005, vol. 59 (2), pp. 145–153. DOI: 10.1098/rsnr.2004.0082.

3. Jia J., Ding X., Qin Z., Ruan Z., Li W., Liu X., Li H. Overview and analysis of MEMS Coriolis vibratory ring gyroscope. *Measurement*, 2021, vol. 182, p. 109704. DOI: 10.1016/j.measurement.2021.109704.

4. Zhou X., Wu Y., Wu X., Zhang Y., Zheng Y. A novel ring vibrating gyroscope based on side piezo-electrodes. *Journal of Central South University*, 2016, vol. 23, pp. 555–561. DOI: 10.1007/s11771-016-3102-4.

5. Guo X., Cui R., Yan S., Cai Q., Wei W., Shen C., Cao H. Design and experiment for N = 3 wineglass mode metal cylindrical resonator gyroscope closed-loop system. *Electronics*, 2023, vol. 12, p. 131. DOI: 10.3390/electronics12010131.

6. Lin Z., Fu M., Deng Z., Liu N., Liu H. Frequency split elimination method for a solid-state vibratory angular rate gyro with an imperfect axisymmetric-shell resonator. *Sensors*, 2015, vol. 15, pp. 3204–3223. DOI: 10.3390/s150203204.

7. Matveev V.V., Khomyachkova A.N., Kalikanov A.V., Streltsov D.S. Perspektivnye datchiki parametrov dvizheniya, osnovannye na inertsii stoyachikh voln [Advanced motion parameter sensors based on standing wave inertia]. *Pribory i metody izmerenii = Devices and Methods of Measurements*, 2025, vol. 16, no. 4, pp. 294–305. DOI: 10.21122/2220-9506-2025-16-4-294-305.

8. Harris B. The influence of some solutes on Young's modulus of niobium. *Journal of the Less Common Metals*, 1967, vol. 12 (3), pp. 247–250. DOI: 10.1016/0022-5088(67)90121-X.

9. NI-SPAN-C alloy 902 Data Sheet. Publication Number SMC-086. Special Metals Corporation, 2004. 30 p. Available at: https://www.specialmetals.com/documents/technical-bulletins/ni-span-c-alloy-902.pdf (accessed 12.09.2025).

10. Kim H.Y., Wei L., Kobayashi S., Tahara M., Miyazaki S. Nanodomain structure and its effect on abnormal thermal expansion behavior of a Ti-23Nb-2Zr-0.7Ta-1.2O alloy. *Acta Materialia*, 2013, vol. 61 (13), pp. 4874–4886. DOI: 10.1016/j.actamat.2013.04.060.

11. Yang Y., Castany P., Cornen M., Prima F., Li S.J., Hao Y.L., Gloriant T. Characterization of the martensitic transformation in the superelastic Ti-24Nb-4Zr-8Sn alloy by in situ synchrotron X-ray diffraction and dynamic mechanical analysis. *Acta Materialia*, 2015, vol. 88, pp. 25–33. DOI: 10.1016/j.actamat.2015.01.039.

12. Zhang L., Wang D., Ren X., Wang Y. A new mechanism for low and temperature-independent elastic modulus. *Scientific Reports*, 2015, vol. 5, p. 11477. DOI: 10.1038/srep11477.

13. Deng Z., Chu K., Li Q., Onuki Y., Sun Q. Elinvar property of cold-rolled NiTi alloy. *Scripta Materialia,* 2020, vol. 187, pp. 197–201. DOI: 10.1016/j.scriptamat.2020.05.058.

14. Saito T., Furuta T., Hwang J.H., Kuramoto S., Nishino K., Suzuki N., Chen R., Yamada A., Ito K., Seno Y., Nonaka T., Ikehata H., Nagasako N., Iwamoto C., Ikuhara T., Sakuma T. Multifunctional alloys obtained via a dislocation-free plastic deformation mechanism. *Science*, 2003, vol. 300 (5618), pp. 464–467. DOI: 10.1126/science.1081957.

15. Niinomi M. Mechanical biocompatibilities of titanium alloys for biomedical applications. *Journal of the Mechanical Behavior of Biomedical Materials*, 2008, vol. 1 (1), pp. 30–42. DOI: 10.1016/j.jmbbm.2007.07.001.

16. Wagner M.F.-X., Windl W. Lattice stability, elastic constants and macroscopic moduli of NiTi martensites from first principles. *Acta Materialia*, 2008, vol. 56 (20), pp. 6232–6245. DOI: 10.1016/j.actamat.2008.08.043.

17. Qiu S., Krishnan V.B., Padula S.A., Noebe R.D., Brown D.W., Clausen B., Vaidyanathan R. Measurement of the lattice plane strain and phase fraction evolution during heating and cooling in shape memory NiTi. *Applied Physics Letters,* 2009, vol. 95 (14), p. 141906. DOI: 10.1063/1.3245308.

18. Stebner A.P., Gao X., Brown D.W., Brinson L. Neutron diffraction studies and multivariant simulations of shape memory alloys: Empirical texture development–mechanical response relations of martensitic nickel–titanium. *Acta Materialia*, 2011, vol. 59 (7), pp. 2841–2849. DOI: 10.1016/j.actamat.2011.01.023.

19. Stebner A.P., Brown D.W., Brinson L. Young's modulus evolution and texture-based elastic–inelastic strain partitioning during large uniaxial deformations of monoclinic nickel–titanium. *Acta Materialia,* 2013, vol. 61 (6), pp. 1944–1956. DOI: 10.1016/j.actamat.2012.12.015.

20. Qin F., Lu F., Chen Y., Yang J., Zhao X. Deformation induced Elinvar behavior in Fe-Ni Invar alloy. *Science Bulletin*, 2018, vol. 63 (16), pp. 1040–1042. DOI: 10.1016/j.scib.2018.07.006.

21. Ahadi A., Khaledialidusti R., Kawasaki T., Harjo S., Barnoush A., Tsuchiya K. Neutron diffraction study of temperature-dependent elasticity of B19′ NiTi-Elinvar effect and elastic softening. *Acta Materialia*, 2019, vol. 173, pp. 281–291. DOI: 10.1016/j.actamat.2019.05.027.

22. Song Y.W., Jin M., Zuo S., Jin X. Elinvar effect in severely-deformed Ti-50.8(at%)Ni thin belt. *Materials Letters*, 2019, vol. 252, pp. 96–99. DOI: 10.1016/j.matlet.2019.05.109.

23. Dubinskiy S.M., Markova G.N., Yudina E., Prokoshkin S.D., Brailovski V. Elinvar effect in thermomechanically treated Ti-Nb-Zr alloy. *ESOMAT 2018 – European Symposium on Martensitic Transformations*. Invited Articles from ESOMAT 2018. 2019, p. 83. DOI: 10.1051/esomat/201900083.

24. Dubinskiy S., Markova G., Baranova A., Vvedenskiy V., Minkova I., Prokoshkin S.D., Brailovski V. A non-typical Elinvar effect on cooling of a beta Ti-Nb-Zr alloy. *Materials Letters,* 2022, vol. 314, p. 131870. DOI: 10.1016/j.matlet.2022.131870.

25. Baranova A., Dubinskiy S., Tabachkova N., Prokoshkin S., Brailovski V. Kinetic features of the isothermal ω-phase formation in superelastic Ti-Nb-Zr alloys. *Materials Letters*, 2022, vol. 325, p. 132820. DOI: 10.1016/j.matlet.2022.132820.

26. Baranova A., Dubinskiy S., Konopatsky A., Markova G., Vvedenskaia I., Prokoshkin S., Brailovski V. On the mechanisms and thermocyclic stability of $\beta \rightarrow \omega_{iso}$ transformation in a superelastic Ti–Nb–Zr shape memory alloy. *Shape Memory and Superelasticity,* 2024, vol. 10 (3), pp. 289–296. DOI: 10.1007/s40830-024-00497-7.

27. Kim H.Y., Miyazaki S. Martensitic transformation and superelastic properties of Ti-Nb based alloys. *Materials Transactions,* 2015, vol. 56 (5), pp. 625–634. DOI: 10.2320/matertrans.M2014454.

28. Dubinskiy S., Baranova A., Markova G., Prokoshkin S. Search for intrinsic elinvar behaviour in beta titanium alloys. *Materials Letters*, 2024, vol. 366, p. 136504. DOI: 10.1016/j.matlet.2024.136504.

29. Murray J.L. The Ti-Zr system. Murray J.L. *Phase diagrams of binary titanium alloys*. Metals Park, Ohio, ASM International, 1987, pp. 340–345.

30. Martins G., da Silva C., Nunes C., Trava-Airoldi V., Borges L.A., Machado J.P.B. Beta Ti-45Nb and Ti-50Nb alloys produced by powder metallurgy for aerospace application. *Materials Science Forum*, 2010, vol. 660–661, pp. 405–410. DOI: 10.4028/www.scientific.net/MSF.660-661.405.

31. Kim H.Y., Hashimoto S., Kim J.I., Hosoda H., Miyazaki S. Mechanical properties and shape memory behavior of Ti-Nb alloys. *Materials Transactions*, 2004, vol. 45 (7), pp. 2443–2448. DOI: 10.2320/matertrans.45.2443.

32. Kim H.Y., Kim J.I., Inamura T., Hosoda H., Miyazaki S. Effect of thermo-mechanical treatment on mechanical properties and shape memory behavior of Ti-(26-28) at.% Nb alloys. *Materials Science and Engineering: A,* 2006, vol. 438–440, pp. 839–843. DOI: 10.1016/j.msea.2006.02.136.

33. Afonso C., Aleixo G., Ramirez A., Caram R. Influence of cooling rate on microstructure of Ti–Nb alloy for orthopedic implants. *Materials Science and Engineering: C*, 2007, vol. 27 (4), pp. 908–913. DOI: 10.1016/j.msec.2006.11.001.

34. Karre R., Niranjan M.K., Dey S.R. First principles theoretical investigations of low Young's modulus beta Ti–Nb and Ti–Nb–Zr alloys compositions for biomedical applications. *Materials Science and Engineering: C*, 2015, vol. 50, pp. 52–58. DOI: 10.1016/j.msec.2015.01.061.

35. Baranova A.P. *Strukturnye faktory i termomekhanicheskie usloviya proyavleniya netipichnogo elinvarnogo effekta v splavakh s pamyat'yu formy na osnove Ti-Nb*. Diss. kand. fiz.-mat. nauk [Structural factors and thermomechanical conditions for the manifestation of the non-typical Elinvar effect in Ti-Nb-based shape memory alloys. PhD. in phys. and math. sci. diss.]. Moscow, 2022. 145 p.

36. Brasil S.P. *Análise de parâmetros de influência na microestrutura e propriedades de ligas Ti-Mo-Zr aplicadas em próteses ortopédicas*. PhD Thesis. Campinas, Universidade Estadual de Campinas, 2008. 215 p.

37. Glazunov S.G., Moiseev V.N. *Konstruktsionnye titanovye splavy* [Structural titanium alloys]. Moscow, Metallurgiya Publ., 1974. 368 p.

38. Moiseev V.N. Beta-titanovye splavy i perspektivy ikh razvitiya [Beta-titanium alloys and prospects of their development]. *Metallovedenie i termicheskaya obrabotka metallov = Metal Science and Heat Treatment*, 1998, no. 12, pp. 11–14. (In Russian).

39. Boyer R.R., Briggs R.D. The use of β titanium alloys in the aerospace industry. *Journal of Materials Engineering and Performance*, 2005, vol. 14 (6), pp. 681–685. DOI: 10.1361/105994905X75448.

40. Li M., Min X., Yao K., Ye F. Novel insight into the formation of α″-martensite and ω-phase with cluster structure in metastable Ti-Mo alloys. *Acta Materialia*, 2019, vol. 164, pp. 322–333. DOI: 10.1016/j.actamat.2018.10.048.

41. Weiss I., Semiatin S. Thermomechanical processing of beta titanium alloys – an overview. *Materials Science and Engineering: A*, 1998, vol. 243 (1–2), pp. 46–65. DOI: 10.1016/s0921-5093(97)00783-1.

42. Cardoso F.F., Ferrandini P.L., Lopes E.S.N., Cremasco A., Caram R. Ti–Mo alloys employed as biomaterials: Effects of composition and aging heat treatment on microstructure and mechanical behavior. *Journal of the Mechanical Behavior of Biomedical Materials*, 2013, vol. 32, pp. 31–38. DOI: 10.1016/j.jmbbm.2013.11.021.

43. He F., Yang S., Cao J. Effect of cold rolling and aging on the microstructure and mechanical properties of Ti-Nb-Zr alloy. *Journal of Materials Engineering and Performance*, 2020, vol. 29 (5), pp. 3411–3419. DOI: 10.1007/s11665-020-04810-0.

44. Kudryashova A., Lukashevich K., Derkach M., Strakhov O., Dubinskiy S., Andreev V., Prokoshkin S., Sheremetyev V. Effect of cold drawing and annealing in thermomechanical treatment route on the microstructure and functional properties of superelastic Ti-Zr-Nb alloy. *Materials*, 2023, vol. 16 (14), p. 5017. DOI: 10.3390/ma16145017.

45. Baranova A., Dubinskiy S., Vvedenskaya I., Bazlov A., Tabachkova N., Sheremetyev V., Teplyakova T., Strakhov O., Prokoshkin S. Evolution of structure and texture formation in thermomechanically treated Ti-Zr-Nb shape memory alloys. *Applied Sciences*, 2024, vol. 14 (9), p. 3647. DOI: 10.3390/app14093647.

46. Ozan S., Lin J., Li Y., Zhang Y., Munir K., Jiang H., Wen C. Deformation mechanism and mechanical properties of a thermomechanically processed β Ti–28Nb–35.4Zr alloy. *Journal of the Mechanical Behavior of Biomedical Materials*, 2017, vol. 78, pp. 224–234. DOI: 10.1016/j.jmbbm.2017.11.025.

47. Kim K.M., Kim H.Y., Miyazaki S. Effect of Zr content on phase stability, deformation behavior, and Young's modulus in Ti–Nb–Zr Alloys. *Materials*, 2020, vol. 13, p. 476. DOI: 10.3390/ma13020476.

48. De Araújo R., Donato T., Sousa K., Kuroda P., Grandini C. Unveiling the effect of Mo on the crystal structure of β-BCC, microhardness, elastic modulus, and biocompatibility in titanium alloys. *Journal of Alloys and Compounds Communications*, 2025, vol. 6, p. 100076. DOI: 10.1016/j.jacomc.2025.100076.

49. Min X.H., Emura S., Zhang L., Tsuzaki K. Effect of Fe and Zr additions on ω phase formation in β-type Ti–Mo alloys. *Materials Science and Engineering: A*, 2008, vol. 497 (1–2), pp. 74–78. DOI: 10.1016/j.msea.2008.06.018.

50. GOST 19807–91. *Titan i splavy titanovye deformiruemye. Marki* [State standard 19807–91. Wrought titanium and titanium alloys. Grades]. Moscow, Standartinform Publ., 2006. 15 p.

51. Helth A., Pilz S., Kirsten T., Giebeler L., Freudenberger J., Calin M., Eckert J., Gebert A. Effect of thermomechanical processing on the mechanical biofunctionality of a low modulus Ti-40Nb alloy. *Journal of the Mechanical Behavior of Biomedical Materials*, 2016, vol. 65, pp. 137–150. DOI: 10.1016/j.jmbbm.2016.08.017.

52. Zhou Y.-L., Luo D.-M. Microstructures and mechanical properties of Ti–Mo alloys cold-rolled and heat treated. *Materials Characterization*, 2011, vol. 62 (10), pp. 931–937. DOI: 10.1016/j.matchar.2011.07.010.

53. Chiu W.-T., Hayakawa R., Nohira N., Tahara M., Inamura T., Hosoda H. Correspondence of the aging behaviors and the phase constituents of the Ti-Mo-based alloys tailored by the Al and Zr additions. *Journal of Alloys and Compounds*, 2024, vol. 991, p. 174509. DOI: 10.1016/j.jallcom.2024.174509.

54. Lu J.-W., Zhao Y.-Q., Ge P., Niu H.-Z. Microstructure and beta grain growth behavior of Ti–Mo alloys solution treated. *Materials Characterization*, 2013, vol. 84, pp. 105–111. DOI: 10.1016/j.matchar.2013.07.014.

55. Wang T., Guo H., Tan L., Yao Z., Zhao Y., Liu P. Beta grain growth behaviour of TG6 and Ti17 titanium alloys. *Materials Science and Engineering: A*, 2011, vol. 528 (21), pp. 6375–6380. DOI: 10.1016/j.msea.2011.05.042.

56. Ferreira A.M., Martorano M.A., De Lima N.B., Padilha A.F. Effects of recovery and recrystallization on microstructure and texture during annealing of a cold deformed superconducting Nb-50(wt.)%Ti alloy. *Journal of Alloys and Compounds*, 2021, vol. 887, p. 161334. DOI: 10.1016/j.jallcom.2021.161334.

57. Cai S., Bailey D.M., Kay L.E. Effect of annealing and cold work on mechanical properties of beta III titanium. *Journal of Materials Engineering and Performance*, 2012, vol. 21, pp. 2559–2565. DOI: 10.1007/s11665-012-0302-4.

58. Zhang S., Wang Q., Cheng X., Han J., Zhang W., Zhang C., Wu J. Static recrystallization behavior and texture evolution during annealing in a cold rolling beta titanium alloy sheet. *Metals*, 2022, vol. 12, p. 899. DOI: 10.3390/met12060899.

59. Zhang K., Wang K., Fu Y., Xiao W., Han J., Zhao X. Strain glass transition in a metastable β Ti-Nb-O alloy with high oxygen content. *Scripta Materialia*, 2022, vol. 214, p. 114661. DOI: 10.1016/j.scriptamat.2022.114661.

60. Wang Y., Gao J., Wu H., Yang S., Ding X., Wang D., Ren X., Wang Y., Song X., Gao J. Strain glass transition in a multifunctional β-type Ti alloy. *Scientific Reports*, 2014, vol. 4, p. 3995. DOI: 10.1038/srep03995.

61. Cui J., Ren X. Elinvar effect in Co-doped TiNi strain glass alloys. *Applied Physics Letters*, 2014, vol. 105 (6), p. 061904. DOI: 10.1063/1.4893003.

62. Muradyan A., Lukashevich K., Derkach M., Andreev V., Cheverikin V., Prokoshkin S., Sheremetyev V. Microstructure and properties of superelastic Ti-18Zr-15Nb alloy subjected to combination of moderate/severe cold drawing and post-deformation annealing. *Journal of Alloys and Compounds*, 2024, vol. 1010, p. 177370. DOI: 10.1016/j.jallcom.2024.177370.

63. Lukashevich K., Komissarov A., Andreev V., Prokoshkin S., Sheremetyev V. Comparative study of mechanical and functional properties of age-hardened superelastic Ti–Zr–Nb alloy with different initial microstructures. *Shape Memory and Superelasticity,* 2024, vol. 10, pp. 392–406. DOI: 10.1007/s40830-024-00507-8.

Conflicts of Interest

The authors declare no conflict of interest.